Physica E 85 (2017) 302–307

Contents lists available at ScienceDirect

Physica E

journal homepage: www.elsevier.com/locate/physe

The electronic and magnetic properties of corrugated zigzag graphene nanoribbons with divacancy defects

Xiao-Dong Tan[a], Xiao-Ping Liao[a], Litao Sun[a,b,c,*]

[a] SEU-FEI Nano-Pico Center, Key Laboratory of MEMS of Ministry of Education, Collaborative Innovation Center for Micro/Nano Fabrication, Device and System, Southeast University, Nanjing 210096, People's Republic of China
[b] Center for Advanced Carbon Materials, Southeast University and Jiangnan Graphene Research Institute, Changzhou 213100, People's Republic of China
[c] Center for Advanced Materials and Manufacture, Joint Research Institute of Southeast University and Monash University, Suzhou 215123, People's Republic of China

ARTICLE INFO

Keywords:
Zigzag graphene nanoribbons
Vacancy defect
Corrugation
First principles

ABSTRACT

We investigate the electronic and magnetic properties of the corrugated zigzag graphene nanoribbons (ZGNRs) with divacancy defects by means of the first principle calculations. We show that the magnitude of corrugation in the defective ZGNR determines whether the system is in the antiferromagnetic state, in the ferromagnetic state, or in the nonmagnetic state. Correspondingly, the mutual transition between the semiconductor and the metal can also be realized in this structure. Moreover, for semiconductors the energy gap displays oscillating behaviors as the magnitude of corrugation increases. These results are identified as being useful in manufacturing flexible devices.

1. Introduction

Graphene, a two-dimensional network of carbon atoms, has attracted extensive interest due to its unique physical properties and promising applications in future nanodevices [1]. However, pure graphene is a zero gap semiconductor, which seriously hinders its way to use for logic electronics, thus raising the question of how to effectively tune the energy gap. One of brilliant strategies is to tailor the graphene sheet into zigzag nanoribbons (ZGNRs), which not only modifies the electronic structure but also brings the edge magnetism [2–4]. Such edge magnetism was shown to be very promising for applications in spintronics devices [5–8]. Besides processing the graphene sheet into nanoribbons, chemical doping [9–12], defects [13–15], and mechanical deformations such as strained [16–18], twisted [19], wiggled [20], folded [21], bended [22–24] structures, and graphene corrugations [25], also have significant effects on the electronic and magnetic properties of graphene. Corrugations inhere in the suspended graphene sheet [26], and can also be induced by substrates [27], defects [28], or adsorbates [29]. Such corrugations would lead to a long-range scattering potential in single-layer graphene, and severely modify the charge-carrier mobility [30] as well as spin-orbit couplings and spin relaxation [31]. In graphene nanoribbons (GNRs) [32–35], these corrugations also play a significant role in their electronic band structures [33,34] and transport properties [35]. Thus, understanding of how corrugations modify the electronic and magnetic properties of graphene and GNRs is a very important issue for the basic research.

From the practical standpoint, such knowledge is also very important for graphene's applications in flexible electronics [36], because the corrugations are difficult to avoid. On the one hand, in the process of fabricating graphene-based flexible devices, graphene is always put on a substrate, which may enhance the corrugations in graphene due to the interaction and the lattice mismatch between graphene and substrate surface. On the other hand, mechanical deformations or other factors can also cause graphene corrugations. Recently, numerous graphene-based flexible devices have been widely studied including energy conversion and storage [37–39], transistors [40,41], sensors [42,43], and wearable devices [44,45]. However, the role of corrugations is less considered.

In this paper we study the influences of corrugations on the electronic and magnetic properties of the ZGNR with divacancy defects. These defects might be created in regions of different curvature by

* Corresponding author at: SEU-FEI Nano-Pico Center, Key Laboratory of MEMS of Ministry of Education, Collaborative Innovation Center for Micro/Nano Fabrication, Device and System, Southeast University, Nanjing 210096, People's Republic of China.
E-mail address: slt@seu.edu.cn (L. Sun).

http://dx.doi.org/10.1016/j.physe.2016.09.009
Received 4 July 2016; Received in revised form 16 August 2016; Accepted 19 September 2016
Available online 20 September 2016

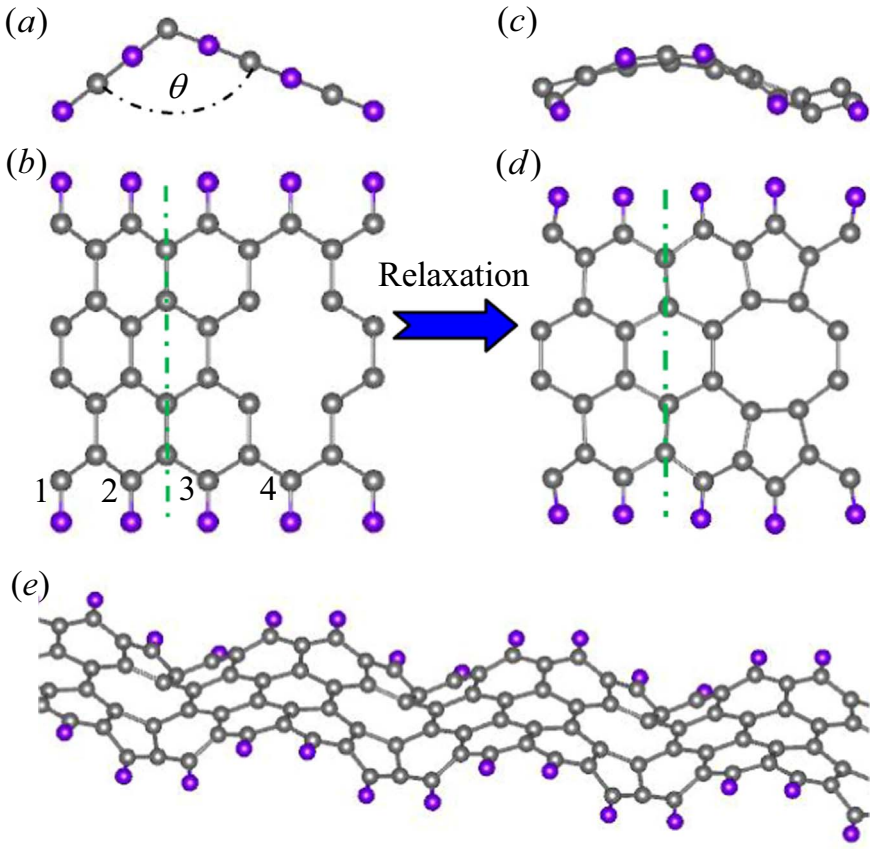

Fig. 1. (a) Side view and (b) top view of original model structural of DV-ZGNR in the periodic supercell. θ is the curvature angle before structure relaxation. (c) Side view and (d) top view of the model structural of DV-ZGNR after full relaxation. (e) Full view of optimized model structure for $\theta = 120^{o}$. The gray and the purple balls represent carbon and hydrogen atoms, respectively. The green line indicates the curved site. (For interpretation of the references to color in this figure legend, the reader is referred to the web version of this article.)

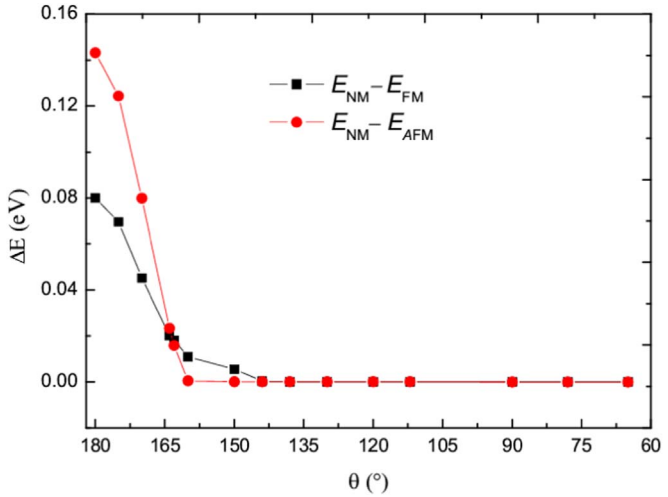

Fig. 2. The energy difference per supercell between the NM and the FM (AFM) state as a function of the curvature angle θ.

using a focused electron beam [46]. As we all know, vacancies can induce magnetic moment [47,48], and modify the electronic and phonon properties of graphene [49]. Moreover, the magnetism of vacancies in corrugated graphene can be controlled by altering the magnitude of corrugation under isotropic strain [50]. In the present work, we mainly focus on the role of the magnitude of corrugation. We will show that when the magnitude of corrugation increases the electronic property of ZGNR with divacancy defects experiences a semiconductor-metal-semiconductor transition, while for the magnetic property the system exhibits an antiferromagnetic-ferromagnetic-nonmagnetic phase transition. We further show that the energy gap displays oscillating behaviors when the system is tuned to the nonmagnetic state.

2. Model and method

The original structure was constructed by asymmetrically bending the ZGNR with double-vacancy defects in the periodic supercell. For convenience, this ribbon is denoted by DV-ZGNR. The degree of initial curvature is characterized by angle θ [see Fig. 1(a)], which determines the magnitude of corrugation when the curved site is fixed [see the green dashed line in Fig. 1(b)]. The double-vacancy locates in the vicinity of the border region of the supercell, and all the edge carbon atoms are saturated by hydrogen atoms to avoid dangling bonds.

Our calculations were performed in the framework of the spin-polarized density functional theory (DFT), as implemented in the plane-wave-basis-set VASP code [51]. The generalized gradient approximation (GGA) of Perdew-Burke-Ernzerhof (PBE) form [52] was employed to describe the exchange-correlation term. The core electrons were treated with projector augmented wave (PAW) potentials [53]. The plane wave cutoff energy was set to 500 eV, and further increasing this value had little effect on the results. The structures were relaxed until the energy and force on each atom were less than 10^{-6} eV and

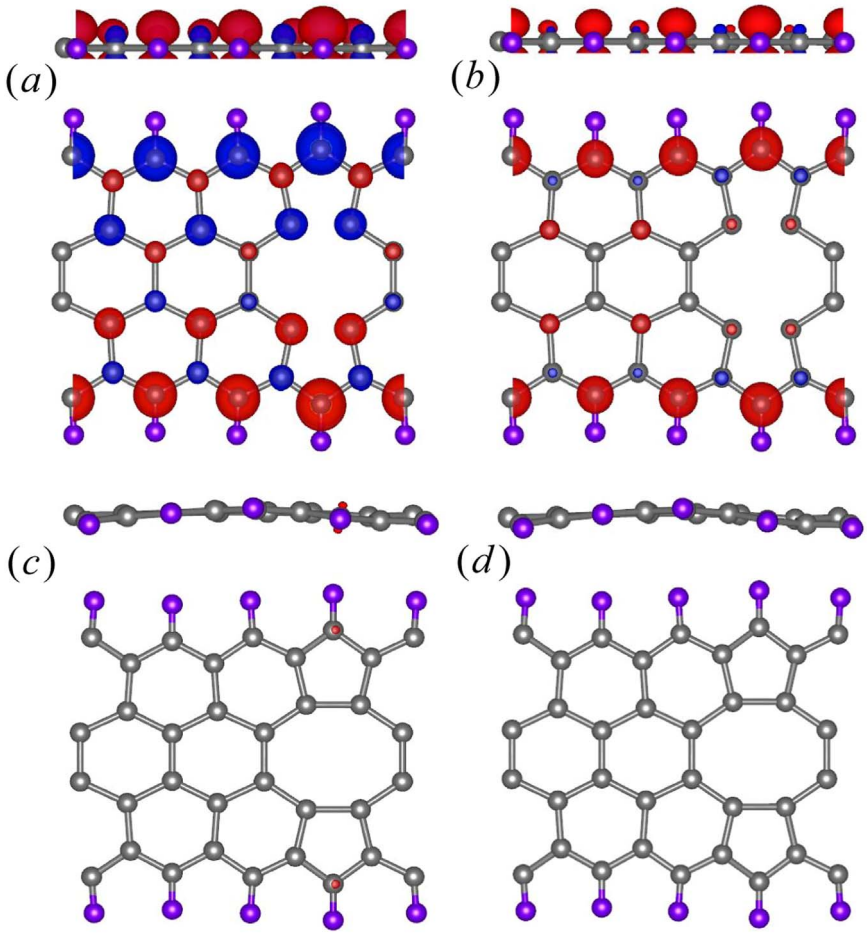

Fig. 3. Side view (upper) and top view (lower) of the spatial spin density distribution for (a) 164°-DV-ZGNR, (b) 163°-DV-ZGNR, (c) 142°-DV-ZGNR and (d) 141°-DV-ZGNR. The isovalues for red and blue isosurfaces are 0.003 e/Å^3 and −0.003e/Å^3, respectively. (For interpretation of the references to color in this figure legend, the reader is referred to the web version of this article.)

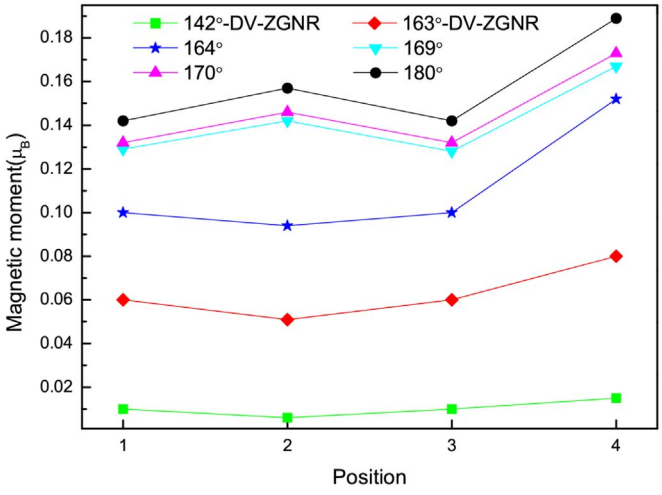

Fig. 4. Local magnetic moments on each carbon atom at the lower edge of corrugated DV-ZGNRs. The position of each lower-edge carbon atom is shown in Fig. 1(b).

0.01 eV/Å, respectively. A 15×1×1 gamma-centered *k*-point mesh was chosen to sample the one-dimensional Brillouin zone. Lower values of smearing (0.01 eV) were used to get the accurate spin configurations for the relaxed structures. To simulate the solo ribbons, both layer-layer and edge-edge distances were kept no less than 15 Å. After full relaxation, the model structure exhibits a wavelike geometry, as illustrated in Figs. 1(c)-(e).

3. Results and discussions

It is well known that flat pristine ZGNRs have two stable edge states [4,54]. One is the ferromagnetic (FM) state, and another is the antiferromagnetic (AFM) state. In order to determine the stable ground state of the corrugated DV-ZGNR, the spin-polarized total energy calculations were performed for different magnetic phases including nonmagnetic (NM), FM, and AFM configurations. Fig. 2 shows the energy difference per supercell between the nonmagnetic state and the magnetic state (both AFM and FM) as a function of the curvature angle θ. We found that the energy of AFM state is lower than the corresponding FM state when $164^o \leq \theta \leq 180^o$, indicating that AFM state is stable in this range. As the curvature degree increases, the system becomes ferromagnetic near the critical point $\theta = 163^o$. Continuously bending the ZGNR, the system gradually transforms into a NM state. When $\theta < 142^o$, the magnetism completely vanishes, and further curving does not change the NM state even though $\theta = 65^o$. Thus, we found a corrugation-induced magnetism transition from AFM state to FM state and then to NM state in the DV-ZGNRs.

In order to illustrate this phenomenon, we calculated the spin densities of systems in ground state after full relaxation. For conve-

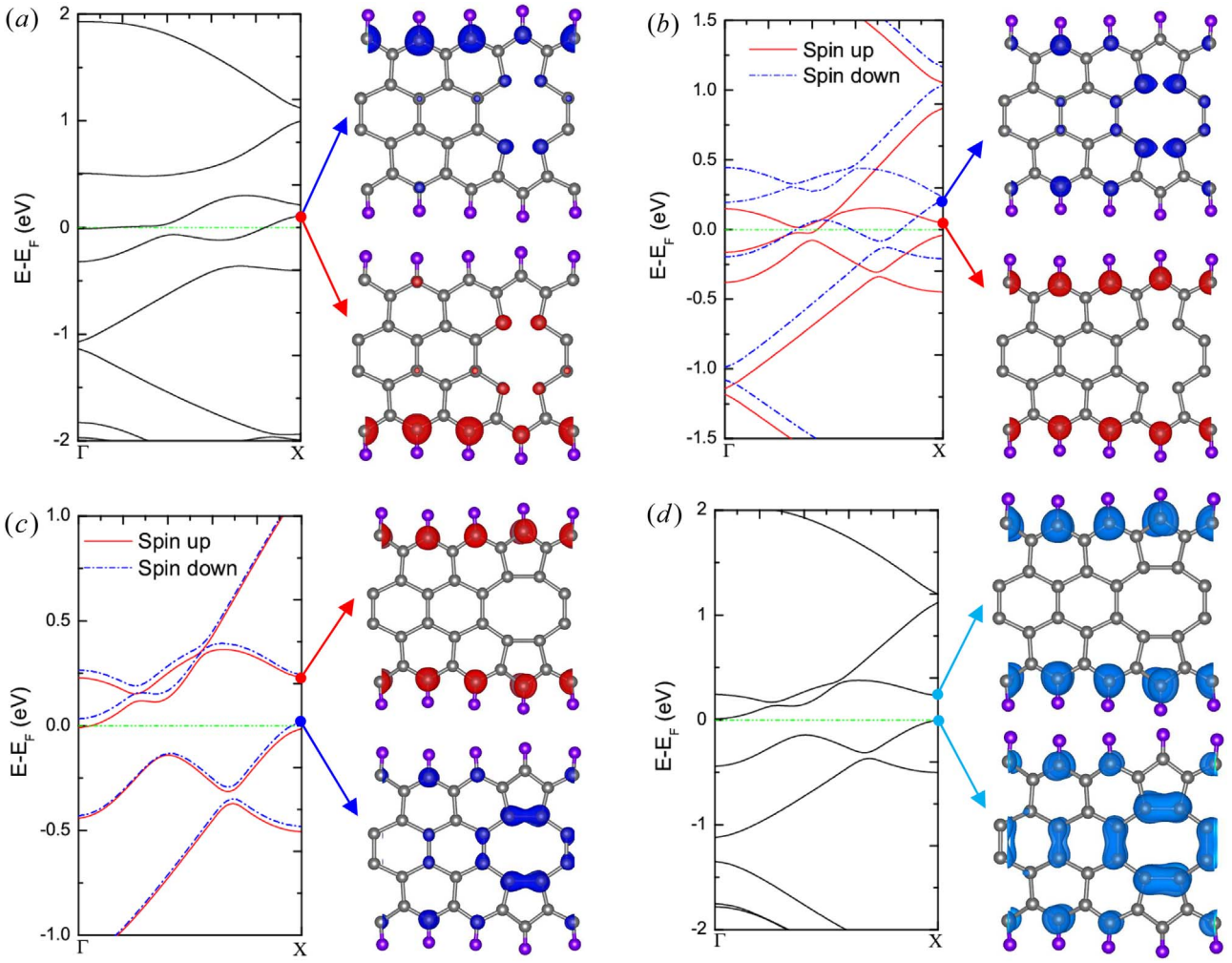

Fig. 5. Band structures of θ-DV-ZGNRs and the corresponding charge densities of the states near the Fermi level at the X point for (a) 164°-DV-ZGNR, (b) 163°-DV-ZGNR, (c) 142°-DV-ZGNR, and (d) 141°-DV-ZGNR. The red solid line and blue dashed line denote spin-up and spin down subbands, respectively. The Fermi level is indicated by a horizontal green dashed line. The isovalue is set to be 0.003 e/Å^3. (For interpretation of the references to color in this figure legend, the reader is referred to the web version of this article.)

nience, the different corrugated DV-ZGNRs are denoted by θ-DV-ZGNRs in this paper. Fig. 3(a) shows the spin distribution of 164°-DV-ZGNR, which is FM coupled along each edge and AFM coupled between the opposite two edges, similar to that of the flat ZGNR. It also shows that the spin density almost distributes in the whole DV-ZGNR and decays from its edges to middle. Fig. 3(b) presents the FM spin density of 163°-DV-ZGNR, which mostly localizes on the two edges and also decays towards to the middle of the ribbon. For 142°-DV-ZGNR, the spin distribution is entirely restricted to the two edge carbon atoms across the double vacancy, as shown in Fig. 3(c). For 141°-DV- ZGNR, we can see that the spin density completely disappears and the system becomes nonmagnetic, as shown in Fig. 3(d). Comparing the spin density distributions for different θ-DV-ZGNRs, we found that the spin density of the edge-site carbon atom adjacent to the double vacancy is locally higher than that of other sites [see Figs. 3(a)–(c)]. The corresponding changes of the local magnetic moments on lower-edge carbon atoms during the corrugation are shown Fig. 4. Obviously, the carbon atomic magnetic moments decrease monotonically with increasing curvature angle.

Besides the magnetic transformation, we also analyzed electronic properties of the corrugated DV-ZGNR. The spin-polarized band structures and the corresponding charge densities at the X point (named as X states) were calculated for different corrugated configurations. Fig. 5(a) shows the band structure of 164°-DV-ZGNR, which displays a metallic character. It clearly shows that the opposite spin-orientation states are degenerate for all subbands. The charge density analysis indicates that the spin-up X states are mostly localized on one edge of the ribbon, while a few states are located in the vicinity of the divacancy. The same behavior is also found in the spin-down X states. For 163°-DV-ZGNR (142°-DV- ZGNR), the system still presents a metallic character, as shown in Fig. 5(b) [Fig. 5(c)]. The corresponding spin-up states at the X point are localized to the edges of the ribbon, while the spin-down X states are mainly located in the vicinity of the divacancy and a few of them are localized on some edge carbon (C) atoms. In the case of 141°-DV-ZGNR, the system exhibits the NM ground state and has a semiconductive character with energy gap of 0.334 eV. We can see in Fig. 5(d) that the lower unoccupied states come from the contribution of edge C atoms, whereas the highest occupied states are mainly attributed to the C atoms near divacancy.

Fig. 6 shows the projected density of states (PDOSs) for all the lower-edge C atoms of the corrugated DV-ZGNRs. It is well-known that the density of states at flat pristine ZGNRs edges may be peaked near the Fermi level due to the presence of localized-edge states. The same behavior is also found in the corrugated DV-ZGNRs. Our results show that the PDOSs are almost composed of p-type states for all the considered systems. In other words, the p-type states are the main contributors to edge states. As can be seen in Figs. 6(a)–(c), the PDOS is continuous around the Fermi lever for both spin channels. This

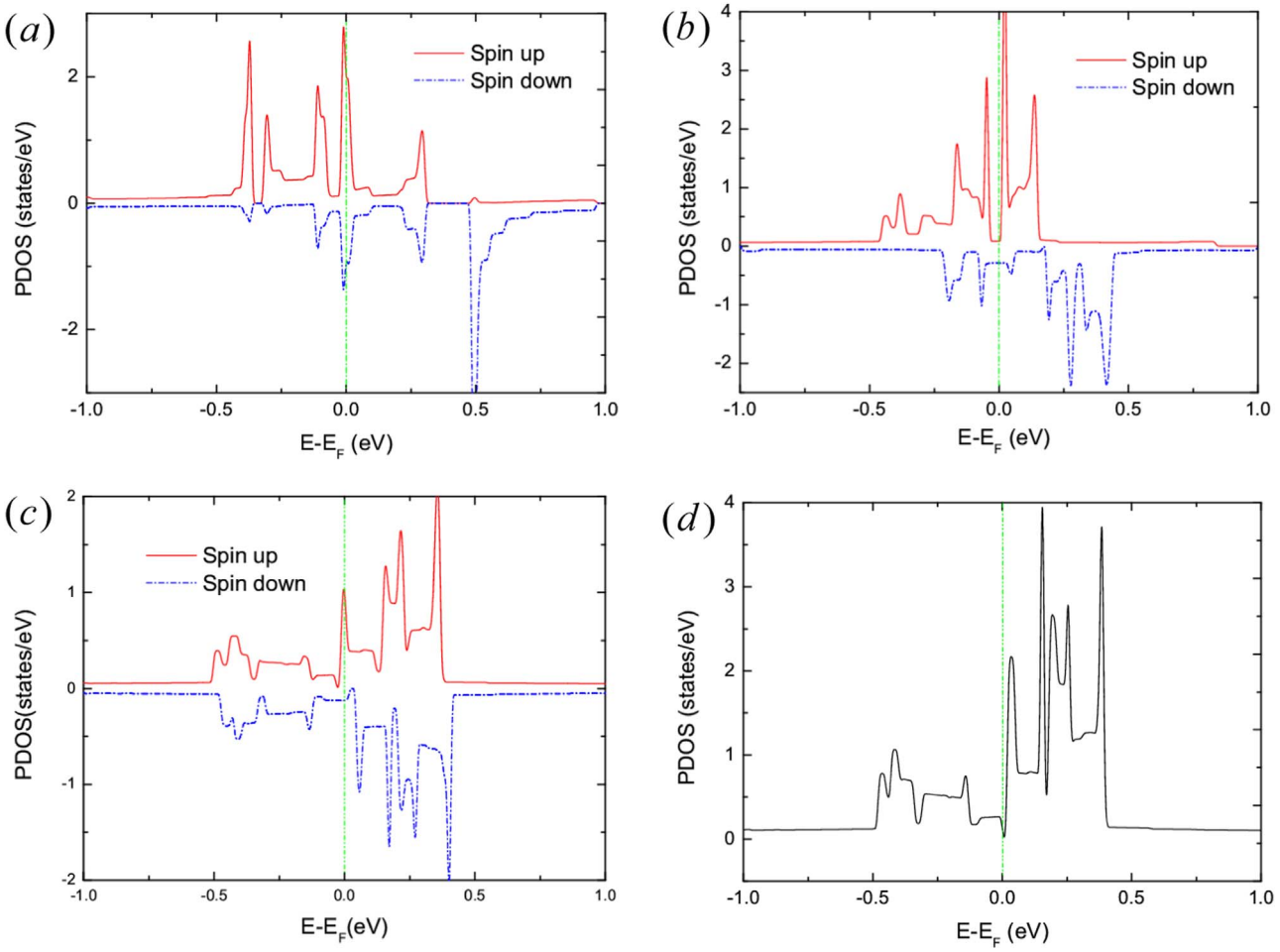

Fig. 6. PDOSs for all the lower-edge carbon atoms of (a) 164°-DV-ZGNR, (b) 163°-DV-ZGNR, (c) 142°-DV-ZGNR, and (d) 141°-DV-ZGNR. The positive red line and the negative blue line represent spin-up and spin-down channels, respectively. (For interpretation of the references to color in this figure legend, the reader is referred to the web version of this article.)

Table 1
Magnetic phase and electronic character of the DV-ZGNRs at different initial curvature angles after full relaxation. M and S denote metal and semiconductor, respectively.

Degree of curvature	Magnetism	Electronic character
$65^o \le \theta \le 141^o$	NM	S
$142^o \le \theta \le 163^o$	FM	M
$164^o \le \theta \le 169^o$	AFM	M
$170^o \le \theta \le 180^o$	AFM	S

behavior indicates that the system displays the metallic character, consistent with the above analysis of the band structure. For 141°-DV-ZGNR, the system is not spin polarized, and the zero PDOS at the Fermi lever illustrates that the system is a zero gap semiconductor, as shown in Fig. 6(d). These results indicate that the electronic structure of the DV-ZGNR can be effectively modified by the small-magnitude corrugation.

To get further insight into the electronic properties of the system, we also performed the band-structure calculations for more corrugated samples of DV-ZGNRs, and the results were summarized in Table 1. Figs. 7(a)–(d) show the band structures of 168°-DV-ZGNR, 169°-DV-ZGNR, 170°-DV-ZGNR, and 180°-DV-ZGNR, respectively. We can clearly see that the system in the AFM state is highly sensitive to the corrugation, where $\theta = 169^o$ is a critical curvature angle separating the metal character of system from the semiconductive one. For semiconductors, the variation of the energy gap with increasing curvature angle is shown in Fig. 8, and the oscillating behavior is found. The similar behaviors also exist in relatively wide DV-ZGNRs, but the critical curvature angle is changed.

4. Conclusions

We have investigated the electronic and magnetic properties of the corrugated DV-ZGNRs by performing the first principle calculations within the DFT. We found that the system exhibits an AFM-FM-NM phase transition as the magnitude of corrugation increases, where the magnitude is governed by the initial curvature angle θ of DV-ZGNR in the unit supercell. Specifically, the system displays the NM state for $65^o \le \theta \le 141^o$, the FM state for $142^o \le \theta \le 163^o$, and the AFM state for $164^o \le \theta \le 180^o$. Correspondingly, the electronic property of the system experiences a transformation from semiconductor to metal and then back to semiconductor. We also found that the energy gap of the system decreases monotonically for AFM states, and fluctuates with increasing magnitude of corrugation for the NM states. These remarkable properties are mainly attributed to the effect of corrugations in DV-ZGNRs.

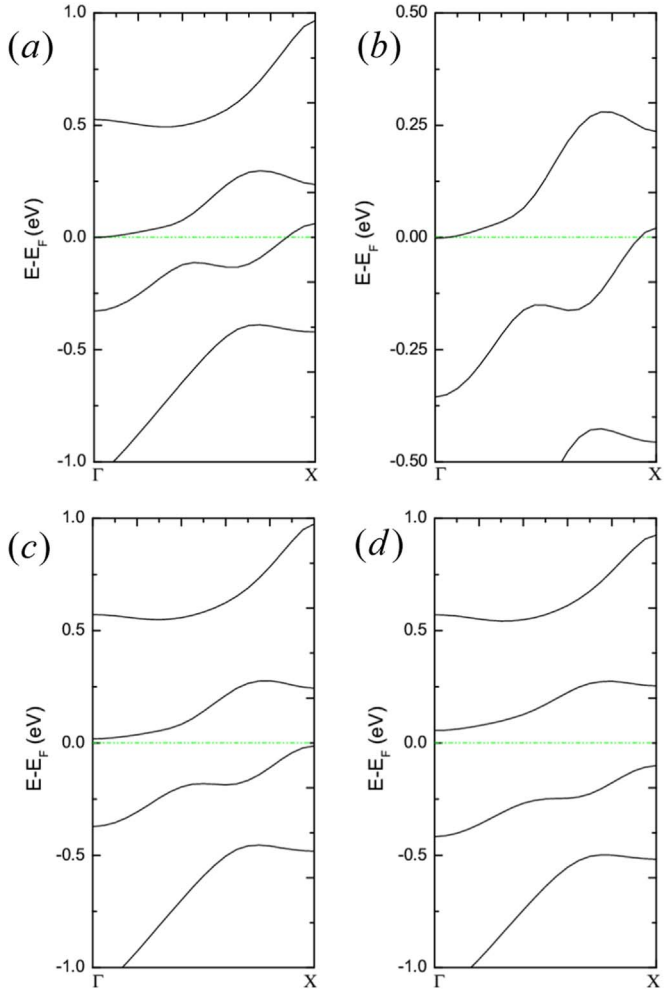

Fig. 7. Band structures of (a) 168°-DV-ZGNR, (b) 169°-DV- ZGNR, (c) 170°-DV-ZGNR,

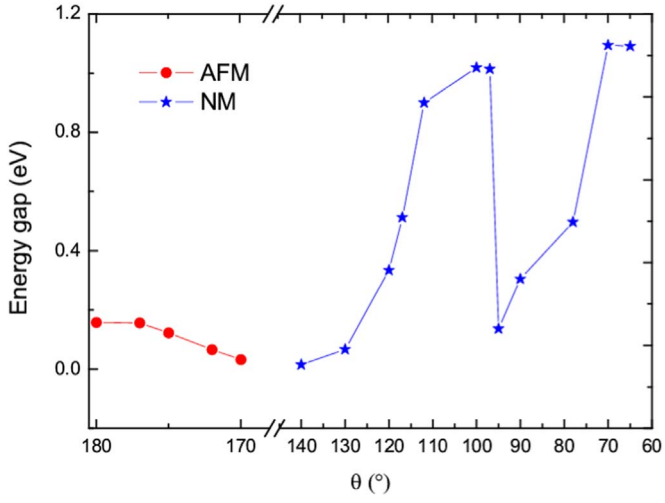

Fig. 8. The energy gap of the DV-ZGNR as a function of the initial curvature angle. The red dot represents the AFM ground state, and the blue star denotes the NM ground state. (For interpretation of the references to color in this figure legend, the reader is referred to the web version of this article.)

Acknowledgments

We acknowledge insightful discussions with Xiaohui Hu. This work was supported by the National Natural Science Foundation of China (Nos. 51420105003, 11327901, 61274114, and 11525415). Computational resources were provided by National Supercomputing Center in Tianjin.

References

[1] A.H. Castro Neto, F. Guinea, N.M.R. Peres, K.S. Novoselov, A.K. Geim, Rev. Mod. Phys. 81 (2009) 109.
[2] K. Nakada, M. Fujita, G. Dresselhaus, M.S. Dresselhaus, Phys. Rev. B 54 (1996) 17954.
[3] M. Fujita, K. Wakabayashi, K. Nakada, K. Kusakabe, J. Phys. Soc. Jpn. 65 (1996) 1920.
[4] Y. Son, M.L. Cohen, S.G. Louie, Phys. Rev. Lett. 97 (2006) 216803.
[5] L. Brey, H.A. Fertig, S.D. Sarma, Phys. Rev. Lett. 99 (2007) 116802.
[6] T. Nikolaos, J. Csaba, P. Mihaita, H.T. Jonkman, B.J.V. Wees, Nature 448 (2007) 571.
[7] O.V. Yazyev, M.I. Katsnelson, Phys. Rev. Lett. 100 (2008) 47209.
[8] H. Wei, R.K. Kawakami, G. Martin, F. Jaroslav, Nat. Nanotechnol. 9 (2014) 794.
[9] S. Dutta, A.K. Manna, S.K. Pati, Phys. Rev. Lett. 102 (2009) 96601.
[10] X.Q. Deng, Z.H. Zhang, G.P. Tang, Z.Q. Fan, M. Qiu, C. Guo, Appl. Phys. Lett. 100 (2012) 63107.
[11] X. Hu, W. Zhang, L. Sun, A.V. Krasheninnikov, Phys. Rev. B 86 (2012) 195418.
[12] X. Hu, N. Wan, L. Sun, A.V. Krasheninnikov, J. Phys. Chem. C 118 (2014) 16133.
[13] T.A.R.L. Humberto, Rep. Prog. Phys. 75 (2012) 62501.
[14] A.V. Pokropivny, Y. Ni, Y. Chalopin, Y.M. Solonin, S. Volz, Phys. Status Solidi 251 (2014) 555.
[15] L. Liu, M. Qing, Y. Wang, S. Chen, J. Mater. Sci. Technol. 31 (2015) 599.
[16] V.M. Pereira, A.H. Castro Neto, Phys. Rev. Lett. 103 (2009) 46801.
[17] O. Cretu, A.V. Krasheninnikov, J.A. Rodríguez-Manzo, L. Sun, R.M. Nieminen, F. Banhart, Phys. Rev. Lett. 105 (2010) 196102.
[18] T. Lehmann, D.A. Ryndyk, G. Cuniberti, Phys. Rev. B 88 (2013) 125420.
[19] G.P. Tang, J.C. Zhou, Z.H. Zhang, X.Q. Deng, Z.Q. Fan, Appl. Phys. Lett. 101 (2012) 23104.
[20] E. Costa Girão, L. Liang, E. Cruz-Silva, A.G.S. Filho, V. Meunier, Phys. Rev. Lett. 107 (2011) 135501.
[21] X.H. Zheng, L.L. Song, R.N. Wang, H. Hao, L.J. Guo, Z. Zeng, Appl. Phys. Lett. 97 (2010) 153129.
[22] W.H. Duan, C.M. Wang, Nanotechnology 20 (2009) 75702.
[23] Z. Yu, L.Z. Sun, C.X. Zhang, J.X. Zhong, Appl. Phys. Lett. 96 (2010) 173101.
[24] X. Hu, L. Sun, A.V. Krasheninnikov, Appl. Phys. Lett. 100 (2012) 263115.
[25] Z. Maciej, J. Phys.: Condens. Matter 26 (2014) 135303.
[26] J.C. Meyer, A.K. Geim, M.I. Katsnelson, K.S. Novoselov, T.J. Booth, S. Roth, Nature 446 (2007) 60.
[27] V.D.P. Al, F. Calleja, B. Borca, P.M. Jr, J.J. Hinarejos, F. Guinea, R. Miranda, Phys. Rev. Lett. 100 (2008) 56807.
[28] U. Bangert, M.H. Gass, A.L. Bleloch, R.R. Nair, J. Eccles, Phys. Status Solidi 206 (2009) 1117.
[29] H.C. Schniepp, K.N. Kudin, J.L. Li, R.K. Prud'Homme, R. Car, D.A. Saville, I.A. Aksay, ACS Nano 2 (2008) 2577.
[30] M.I. Katsnelson, A.K. Geim, Philos. Trans. R. Soc. A 366 (2008) 195.
[31] J.S. Jeong, J. Shin, H.W. Lee, Phys. Rev. B 84 (2011) 195457.
[32] J. Campos-Delgado, Y.A. Kim, T. Hayashi, A. Morelos-Gómez, M. Hofmann, H. Muramatsu, M. Endo, H. Terrones, R.D. Shull, M.S. Dresselhaus, Chem. Phys. Lett. 469 (2009) 177.
[33] S. Costamagna, O. Hernandez, A. Dobry, Phys. Rev. B 81 (2010) 115421.
[34] P. Roman-Taboada, G.G. Naumis, Phys. Rev. B 92 (2015) 35406.
[35] S.B. Touski, M. Pourfath, Can. J. Earth Sci. 103 (2013) 143506.
[36] S.J. Kim, K. Choi, B. Lee, Y. Kim, B.H. Hong, Annu. Rev. Mater. Res. 45 (2015) 63.
[37] M.F. El-Kady, S. Veronica, D. Sergey, R.B. Kaner, Science 335 (2012) 1326.
[38] X. Wang, Energy Environ. Sci. 8 (2015) 790.
[39] Y. Shao, M.F. El Kady, L.J. Wang, Q. Zhang, Y. Li, H. Wang, M.F. Mousavi, R.B. Kaner, Chem. Soc. Rev. 44 (2015) 3639.
[40] D.M. Sun, C. Liu, W.C. Ren, H.M. Cheng, Small 9 (2013) 1188.
[41] B.K. Sharma, J.H. Ahn, Solid State Electron. 89 (2013) 177.
[42] P. Labroo, Y. Cui, Biosens. Bioelectron. 41 (2013) 852.
[43] Z. Wang, M. Shaygan, M. Otto, D. Schall, D. Neumaier, Nanoscale 8 (2016) 7683.
[44] C. Hou, H. Wang, Q. Zhang, Y. Li, M. Zhu, Adv. Mater. 26 (2014) 5018.
[45] Y. Liang, J. Mater. Chem. A 3 (2015) 2547.
[46] J.A. Rodriguezmanzo, F. Banhart, Nano Lett. 9 (2009) 2285.
[47] O.V. Yazyev, L. Helm, Phys. Rev. B 75 (2007) 125408.
[48] K.M. Mccreary, A.G. Swartz, W. Han, J. Fabian, R.K. Kawakami, Phys. Rev. Lett. 109 (2012) 186604.
[49] A.V. Pokropivny, Y. Ni, Y. Chalopin, Y.M. Solonin, S. Volz, Phys. Status Solidi 251 (2013) 555.
[50] E.J.G. Santos, S. Riikonen, D. Sánchez-Portal, A. Ayuela, J. Phys. Chem. C. 116 (2012) 7602.
[51] G. Kresse, J. Furthmüller, Comp. Mater. Sci. 6 (1996) 15.
[52] J.P. Perdew, K. Burke, M. Ernzerhof, Phys. Rev. Lett. 77 (1996) 3865.
[53] P.E. Blöchl, Phys. Rev. B 50 (1994) 17953.
[54] T.B. Martins, R.H. Miwa, A.J.R. Da Silva, A. Fazzio, Phys. Rev. Lett. 98 (2007) 196803.